Bimetallic Nanostructures as Active Raman Markers: Gold-Nanoparticle Assembly on 1D and 2D Silver Nanostructure Surfaces

*Ray Gunawidjaja, Eugenia Kharlampieva, Ikjun Choi, and Vladimir V. Tsukruk**

It is demonstrated that bimetallic silver–gold anisotropic nanostructures can be easily assembled from various nanoparticle building blocks with well-defined geometries by means of electrostatic interactions. One-dimensional (1D) silver nanowires, two-dimensional (2D) silver nanoplates, and spherical gold nanoparticles are used as representative building blocks for bottom-up assembly. The gold nanoparticles are electrostatically bound onto the 1D silver nanowires and the 2D silver nanoplates to give bimetallic nanostructures. The unique feature of the resulting nanostructures is the particle-to-particle interaction that subjects absorbed analytes to an enhanced electromagnetic field with strong polarization dependence. The Raman activity of the bimetallic nanostructures is compared with that of the individual nanoparticle blocks by using rhodamine 6G solution as the model analyte. The Raman intensity of the best-performing silver–gold nanostructure is comparable with the dense array of silver nanowires and silver nanoplates that were prepared by means of the Langmuir–Blodgett technique. An optimized design of a single-nanostructure substrate for surface-enhanced Raman spectroscopy (SERS), based on a wet-assembly technique proposed here, can serve as a compact and low-cost alternative to fabricated nanoparticle arrays.

Keywords:
- gold
- nanostructures
- nanowires
- Raman spectroscopy
- silver

1. Introduction

Silver and gold nanoparticles exhibit interesting optical properties, such as localized surface plasmon resonances (LSPRs) that are tunable with their shape,[1] size,[2] and aggregation,[3] as predicted by theoretical models and well supported experimentally.[4–6] Oscillating plasmons result in a local electromagnetic field along the nanoparticles' surface causing the characteristic Raman bands of organic molecules to be greatly enhanced, which is the fundamental of surface-enhanced Raman spectroscopy (SERS). LSPR within the UV/Vis region occurs when the dimension of the nanostructures is significantly smaller than the wavelength of the exciting electromagnetic radiation, within 5–100 nm.[7–10] The high Raman enhancement demonstrated by Kneipp et al. and Nie et al.,[10] which in turned allow single-molecule detection, was attributed to simultaneously operating long-range electromagnetic and short-range chemical enhancement mechanisms.[11,12] It is now well established that electromagnetic enhancement is best obtained at the interstitial sites between neighboring nanoparticles.[13–15] El-Sayed et al. investigated the plasmon shift for a series of gold nanodisk dimers separated at various distances between 2 and 210 nm.[16] Similarly, Lee et al. showed that changing the silver inter-nanowire gap from 35 to 10 nm increases the SERS intensity by 200-fold.[27]

Exhaustive studies have been undertaken to achieve the optimum SERS enhancement as a function of nanoparticle shape,[17] composition,[18] and configuration.[19,20] In terms of geometrical effect, the strongest SERS effect has been

[*] Prof. V. V. Tsukruk, Dr. R. Gunawidjaja, Dr. E. Kharlampieva, I. Choi
School of Materials Science and Engineering
Georgia Institute of Technology
Atlanta, GA 30332–0245 (USA)
E-mail: vladimir@mse.gatech.edu

Supporting Information is available on the WWW under http://www.small-journal.com or from the author.

DOI: 10.1002/smll.200900688

NANO MICRO small

determined for nanoparticles having sharp features.[21] Further work was focused towards various designs of hybrid nanostructures that are either metallic alloy nanostructures or organic–inorganic hybrids.[7,22] Such a design of hybrid nanostructures exhibits a tunable plasmon resonance frequency.[23] Other examples include Ag/Au core/shell nanoparticles,[24] gold–silica composite nanoparticles,[25] ensembles of gold droplets on silicon nanowires,[26] silver-nanoparticle-decorated single silver nanowires,[27] and gold core/palladium shell nanoparticles.[28] We have previously reported that a silver–gold nanocob structure can function as a one-dimensional (1D) SERS marker. The enhancement exceeds that of isolated silver nanowires by two orders of magnitude.[29] In this design, the gold nanoparticles were assembled onto the surface of silver nanowires with a three-arm $(X\text{-}PEO)_1\text{-}(PS\text{-}Y)_2$ (PEO: polyethylene oxide; PS: polystyrene) star-polymer linker by a combination of esterification and click chemistry. However, this design does not provide a high-density gold nanoparticle, critical for an effective SERS phenomenon.

Herein, we report an alternative approach to the design of bimetallic nanostructures through the Coulombic-driven assembly of charged gold nanoparticles onto other anisotropic nanostructures (silver nanowires and nanoplates), which allows fine control of the spatial arrangement of the nanoparticles and a corresponding enhanced Raman scattering.[30–34] We applied this approach to 1D silver nanowires (AgNWs) and two-dimensional (2D) nanoplates (AgNPls), and demonstrated intriguing anisotropic surface plasmon resonances as well as effective SERS phenomena for organic molecules.

2. Results and Discussion

Scheme 1 illustrates the multistep assembly of positively charged gold nanoparticles (Au:4-dimethylaminopyridine (DMAP)) onto negatively charged 1D AgNW:COOH or negatively charged 2D AgNPl:COOH. In the final step, the hybrid nanostructures are coated with poly(acrylic acid) (PAA) to stabilize them in solution. Without this outer coating the hybrid nanostructures tend to form irreversible aggregates that are not dispersible in solution (details can be found in the Experimental Section). The nanostructures are abbreviated as Ag/Au*n*/PAA, where Ag represents silver nanowire (AgNW) or silver nanoplate (AgNPl) and *n* refers to the relative concentration of gold nanoparticles used in the preparation of the silver–gold hybrid nanostructures (more on this below). The structures are dispersible in methanol or water when subjected to sonication and vortexing.

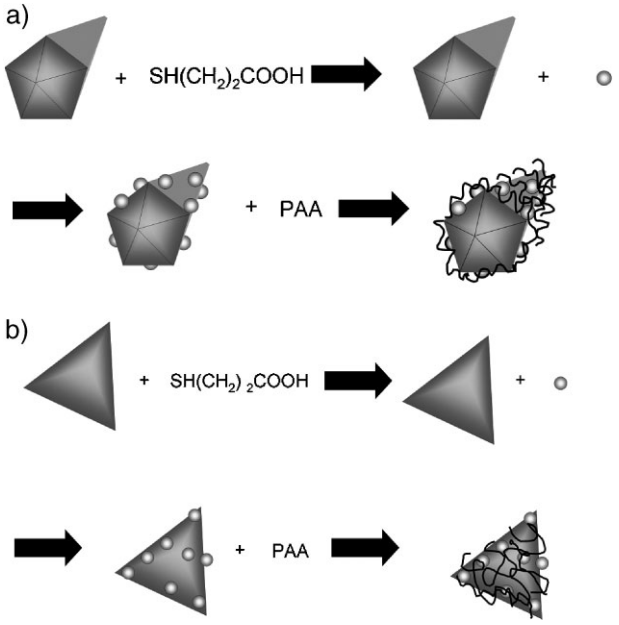

Scheme 1. Assembly of gold nanoparticles onto silver surfaces: a) AgNW/Au/PAA and b) AgNPl/Au/PAA.

2.1. Nanoparticle Building Blocks

The UV/Vis absorption spectra were obtained for each of the purified nanoparticle building blocks in the solution state (Figure 1). Transmission electron microscopy (TEM) images of the initial nanostructure building blocks, that is, 1D AgNW and 2D AgNPl components, are shown in Figure 2. The length of the AgNWs is $L = (6 \pm 2)$ μm with diameter $D = (75 \pm 20)$ nm (aspect ratio, AR = 80). The average height of the AgNPls is (30 ± 10) nm, which exhibits a bimodal width distribution of (190 ± 60) and (470 ± 60) nm. The diameter of the spherical gold nanoparticles is $D = (4.1 \pm 1)$ nm (see Experimental Section).

A characteristic double-peak signature is seen for the UV/Vis spectrum of AgNWs in solution (Figure 1). The peak at 350 nm is due to the quadrupole resonance excitation of nanowires. The other peak at 393 nm is due to transverse plasmon resonance of nanowires, which is proportional to their diameter. According to the linear relation between absorbance maximum and nanowire diameter, which is given by $\lambda_{max} = 361.3 + 0.41 D_{nanowire}$, this peak position corresponds to a diameter of 77 nm as confirmed by atomic force microscopy (AFM) imaging.[35] The longitudinal plasmon peak is not seen within the 200–1000 nm range because of the high-aspect-ratio nanowires,[36] for which it is in the micrometer range.

AgNPls exhibit a similar double-peak resonance spectrum as AgNWs with the addition of a broad band that peaks at 890 nm. Due to their 2D shape, AgNPls can have in-plane and

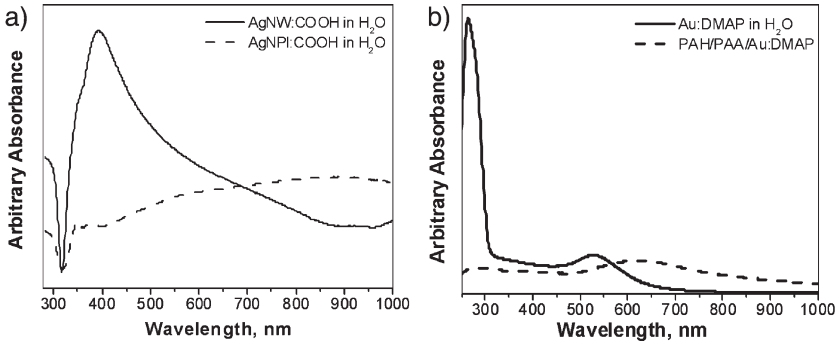

Figure 1. UV/Vis absorption spectra of a) AgNW:PVP and AgNPl:PVP core, and b) Au:DMAP in solution and on PAH/PAA support.

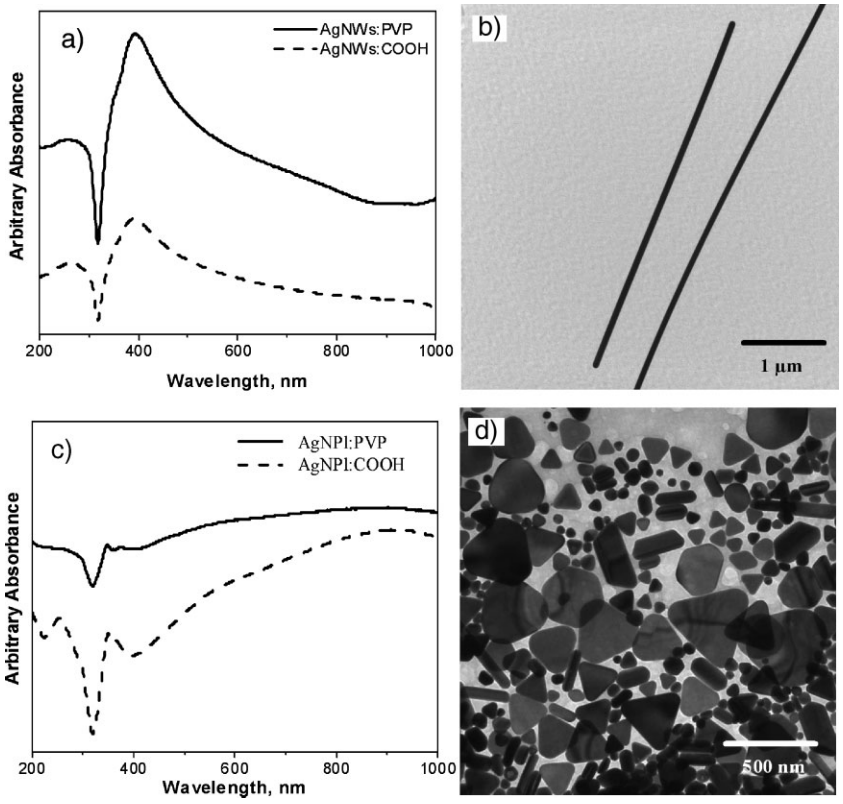

Figure 2. UV/Vis spectra of a) as-synthesized silver nanowires, AgNWs:PVP, and 3-mercaptopropionic acid-functionalized silver nanowires, AgNWs:COOH, and of c) as-synthesized silver nanoplates, AgNPls:PVP, and 3-mercaptopropionic acid-functionalized silver nanoplates, AgNPls:COOH. b,d) The corresponding TEM images of AgNWs and AgNPls, respectively.

2.2. Absorption Spectra of Silver–Gold-Nanoparticle Hybrid Nanostructures

Figure 2 and Figure 3 present the UV/Vis absorption spectra of the silver nanostructures as they undergo modification. Surface modification with 3-mercaptopropanoic acid causes the quadrupole peak to blue-shift in the case of AgNWs, from 393 to 388 nm (Figure 2a). Likewise, the quadrupole resonance peak of AgNPls blue-shifts from 376 to 366 nm following the ligand-exchange procedure. Upon the introduction of gold nanoparticles, the formed silver–gold hybrid nanostructures exhibit a combined resonance spectrum, as previously reported for the hybrid silver–gold nanocobs.[29] By comparing Figure 3 with Figure S2 (Supporting Information), it can be seen that the plasmon peak position due to the gold nanoparticles is further red-shifted for the higher-density gold nanoparticles. AFM and TEM images show the different densities of gold nanoparticles in the two samples (Figure 3, Figure S2).

To further understand the plasmon interaction between the gold nanoparticles and AgNWs, UV/Vis measurement of individual silver–gold nanowires on a quartz substrate was performed (Figure 4 and Figure S3, Supporting Information). Under such experimental conditions, the overall shape of the UV/Vis absorption spectrum of a randomly oriented array of AgNW/Au1/PAA is comparable with that in the solution state (Figure 4a). The characteristic peaks belonging to silver and

out-of-plane dipole and quadrupole resonances. The peak at 350 nm can be assigned to a weak dipole out-of-plane resonance and the peak at 377 nm is assigned to a weak quadrupole out-of-plane resonance (Figure 1a).[1,37] Due to the wide distribution in nanoplate dimensions and shape, the in-plane and out-of-plane quadrupole resonances give rise to a broad halo between 400 and 1000 nm; the dipolar in-plane resonance mode red-shifts with increasing nanodisk diameter. Finally, for the DMAP-modified gold nanoparticles (Au:DMAP), two prominent peaks are seen (Figure 1b). The first peak at 264 nm is indicative of the pyridinium ring from the 4-DMAP molecule and the other peak at 530 nm belongs to the dipole plasmon resonance of the gold nanoparticle. The absorption spectrum of Au:DMAP in the solid state (adsorbed onto a polyallylamine hydrochloride (PAH)/PAA substrate) reveals only a single peak at 623 nm, which indicates that the strong red shift is mainly due to strong interparticle interactions.[38,39] The AFM topographical image reveals that the adsorbed gold nanoparticles appear to be uniform, but occasional aggregates are seen (Figure S1, Supporting Information).

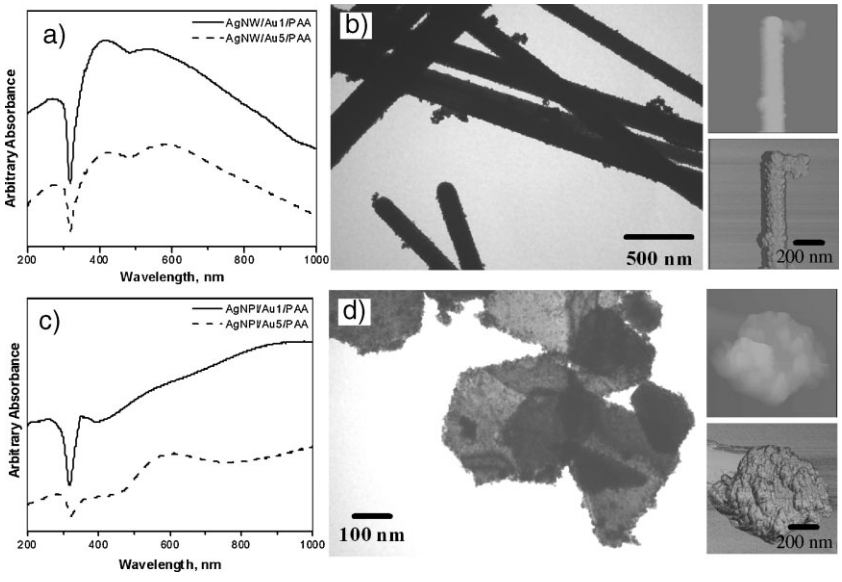

Figure 3. UV/Vis absorption spectra of a) AgNW/Au*n*/PAA and c) AgNPl/Au*n*/PAA ($n = 1$ and 5). b,d) The corresponding TEM (left) and AFM (right) images of AgNW/Au5/PAA and AgNPl/Au5/PAA (height ($z = 200$ nm) (top) and phase images (bottom)).

NANO MICRO small

gold nanoparticles occur at 421 nm, and at 531 and 760 nm, respectively. In this case, the quadrupole resonance peak is absent and the transverse plasmon peak has shifted significantly from 393 nm, as a result of interaction between nanowires due to aggregation and difference in the dielectric environment. The plasmon peak due to gold at 531 nm is consistent with a noninteracting state, whereas the plasmon peak at 760 nm suggests nanoparticle-to-nanoparticle plasmon coupling. For the higher-density gold nanoparticles, AgNW/Au5/PAA, the plasmon peaks due to gold nanoparticles are more red-shifted at 571 and 725 nm (Figure S3a, Supporting Information). This is consistent with increased nanoparticle-to-nanoparticle plasmon coupling (Figure 3).

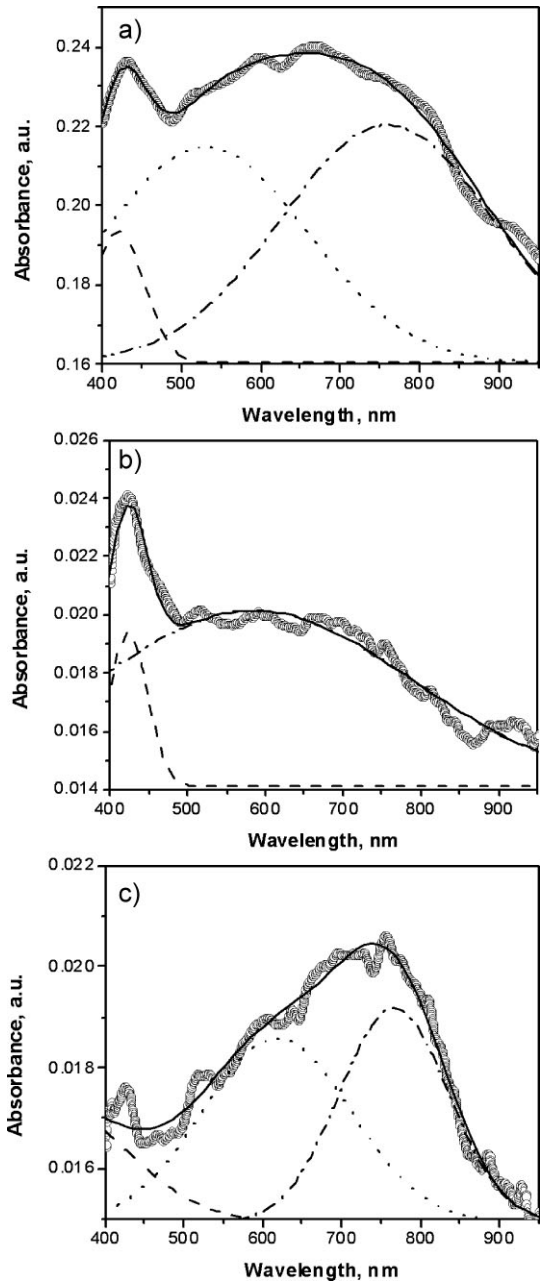

Figure 4. UV/Vis absorption spectra of AgNW/Au1/PAA: a) randomly oriented array deposited on substrate; absorption spectra from a single nanowire measured with polarized excitation light perpendicular to (b) and along (c) the long axis, with the corresponding deconvolution of different peaks. Similar measurements for higher concentrations are presented in the Supporting Information, Figure S3.

UV/Vis measurement of a single silver–gold nanowire with polarized light reveals a significant difference in the short and long axes (see Figure 4b,c and Figure S3b,c, Supporting Information, for AgNW/Au*n*/PAA, $n = 1$ and 5, respectively).[40] For the AgNW/Au1/PAA nanostructure, the transversal LSPR due to the AgNW is strongly excited at 424 nm accompanied by the resonance peak due to gold nanoparticles at 585 nm (Figure 4b and Figure S4d, Supporting Information). However, only absorption as a result of gold nanoparticle LSPR is seen when the excitation light is polarized along the long axis (broad maximum at around 618 and 767 nm; Figure 4c and Figure S4d, Supporting Information). Compared with the solution case this value is much more red-shifted and can be attributed to localized aggregation in the form of dimers and trimers, which becomes significant in the dry state. A similar trend is seen for AgNW/Au5/PAA, except that in this case the plasmon coupling between gold nanoparticles is more significant due to the higher gold nanoparticle density. This is seen from the more significant red shift in the gold nanoparticle LSPR, $\lambda_{max} = 624$ and 787 nm, when the light excitation is polarized along the long axis (Figure S3c, Supporting Information).

2.3. SERS Phenomenon on Silver–Gold Nanostructures

We selected rhodamine 6G (Rh6G) as the popular model Raman analyte. The peak assignment of Rh6G adsorbed on colloidal silver has been described in detail: 614 cm^{-1} (C–C–C ring in-plane bending); 774 cm^{-1} (C–H in-plane bending); 1129 cm^{-1} (C–H in-plane bending), and 1183, 1310, 1363, 1509, 1572, and 1648 cm^{-1} (aromatic C–C stretching).[41] For silver–gold nanowires we performed two independent measurements with the excitation polarization perpendicular or parallel to the nanowire long axis (Figure 5a,b). It is clear from these data that the Raman intensity is much stronger when the silver–gold nanowire is oriented perpendicular to the laser polarization, as previously reported for silver–gold nanocobs as well as other 1D SERS substrates.[27,42–44]

The SERS spectra are well pronounced for the silver–gold nanoparticles even at very low concentration, $C_0 = 10^{-7}$ M and 5×10^{-5} M for the nanowire core and nanoplate core, respectively (Figure 5). The plot of Raman intensity with respect to Rh6G concentration can be fitted according to the equation previously derived by Hildebrandt et al. to describe Raman enhancement, I_{SERR}, of the equilibrium concentration of Rh6G adsorbed on colloidal silver that is dispersed in a certain Rh6G concentration C_0 (Figure S4, Supporting Information).[45] The fit yields an adsorption energy, G_{ad}, that is within 36–41 kJ mol^{-1}, which indicates a strong affinity of Rh6G molecules with the surface. The corresponding threshold concentration, $K_{s,max}$, is within 1×10^{-5}–2×10^{-5} M. The intensity of the main peak at 1650 cm^{-1} ($C_0 = 10^{-7}$ M) increases from 22 to 110 when AgNW/Au5/PAA is measured with the laser polarization parallel and perpendicular to the nanowire orientation (Figure 5a,b). This increase can be attributed to the

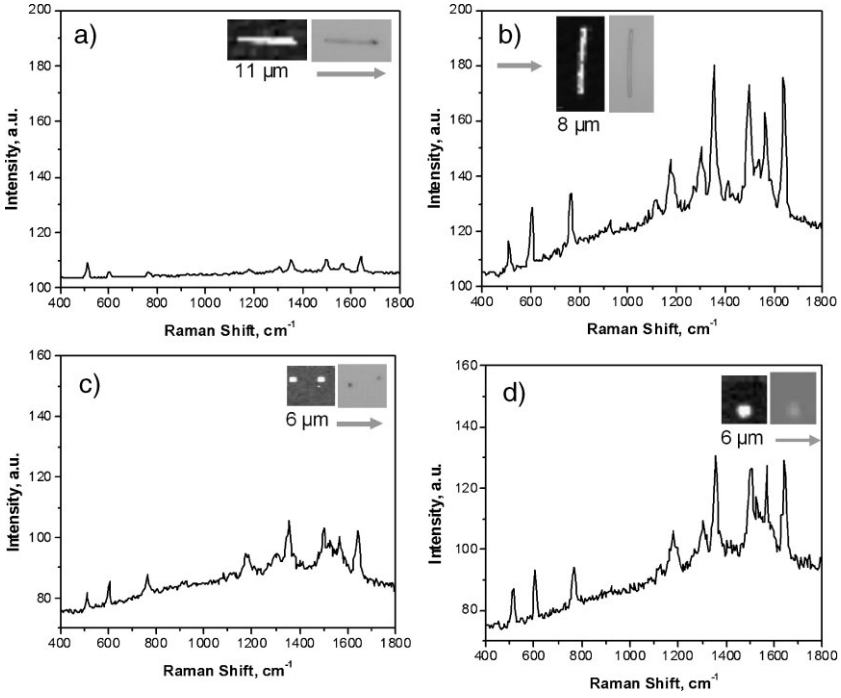

Figure 5. SERS spectra of Rh6G on a) AgNW/Au5/PAA with laser polarized parallel and b) perpendicular to the nanowire orientation (arrows show polarization direction) at $C_0 = 10^{-7}$ M, and c,d) AgNPl/Au*n*/PAA for $n = 1$ (two silver–gold nanoplates) and 5, respectively, at $C_0 = 5 \times 10^{-5}$ M. Insets: Raman intensity mapping within 1630–1680 cm^{-1}, which corresponds to aromatic C–C stretching.

active transverse plasmon resonance of AgNWs enhanced by coupling with the gold nanoparticles, to give an enhanced electromagnetic field when the laser polarization is along the short axis as discussed earlier.

In contrast, plasmon coupling is solely between gold nanoparticles when the laser polarization is along the long axis and results in a lower Raman enhancement. Furthermore, the intensity of the same main peak increases from 10 to 35 counts for AgNPl/Au*n*/PAA when the density of gold nanoparticles is increased (Figure 5c,d). Similarly, the Raman enhancement increases dramatically with increasing gold nanoparticle density on AgNWs (Figure S4, Supporting Information). The silver–gold nanocob can serve as a 1D anisotropic Raman marker capable of detecting the presence of Rh6G down to 10^{-8} M, which is a very low detection limit rarely achieved with Raman-active substrates (Figure 5b).[7]

To further quantify the performance of our single-hybrid-nanoparticle SERS substrate, comparisons were made with dense arrays of AgNWs[48] and AgNPls prepared by the Langmuir–Blodgett technique. Despite a large area of highly ordered and densely packed monolayers of silver nanoparticles, defects in the form of loose-packings or multilayers were occasionally seen (insets of Figures S5a and S5c, Supporting Information). The monolayer films were incubated in 10^{-4} M (saturation concentration) Rh6G for 10 min and Raman mapping within 1630–1680 cm^{-1} was obtained (Figures S5b and S5d, Supporting Information). The Raman mappings show sporadic SERS "hot spots" at the nanoparticle junctions (<10 nm) for AgNWs[46] and likewise for AgNPls, where the hot spots appear in the aggregated regions of interacting nanoplates. This is contrary to the silver–gold hybrid nanoparticle, which uniformly enhances Raman scattering throughout its nanowire or nanoplate surface. Taking the average intensity across the whole area of the Raman map of several locations, under identical conditions the best-performing AgNW/Au5/PAA SERS substrate is on a par with the dense AgNW or AgNPl arrays. The Rh6G intensity at 1650 cm^{-1} is only 20-fold better for the AgNW array and only fivefold better for the AgNPl array. Tao et al. previously estimated that a 1-hexadecanethiol-functionalized AgNW array exhibits a high enhancement factor, $EF = 2 \times 10^9$.[48]

3. Conclusions

A wet-assembly approach of nanoparticles onto 1D and 2D submicrometer nanostructures has been applied to create bimetallic nanostructures having a synergistic optical property. Gold nanoparticles were assembled onto 1D silver nanowires and 2D silver nanoplates. The silver–gold hybrid nanostructures can serve as efficient single-nanoparticle Raman markers. They are capable of trapping organic molecules within the polyelectrolyte matrix and dramatically increasing the SERS phenomenon, which is comparable with that of AgNW arrays. Judicious selection of decorating nanoparticles can lead to a design of SERS substrate that is equal to or better than the AgNW array, which is currently under investigation.

4. Experimental Section

Materials: All chemicals were acquired from Sigma–Aldrich, Alfa–Aesar, VWR, and Fisher and used as received without further purification: silver nitrate salt (99.97%), PVP (number-average molecular weight, $M_n = 1\,300\,000$ g mol^{-1}), ethylene glycol (99%), $Fe(acac)_3$ (acac = acetylacetonate), PAH (70 000 g mol^{-1}), PAA ($M_n = 100\,000$ g mol^{-1}, 35 wt% solution), transparent phosphate buffer (pH 7, 0.05 M), Rh6G, and dimethylformamide (DMF, ACS reagent grade). AgNWs,[47,48] AgNPls,[49] and gold nanoparticles[50] were synthesized in high yield according to standard procedures (see below). In the methods described, PAA solution (2 mg mL^{-1}) in phosphate-buffered solution (0.01 M, pH 7) was used for modification. All associated glassware was cleaned with aqua regia solution (HCl/HNO_3, 3:1; *Caution!*) and rinsed abundantly with Nanopure water.

AgNW synthesis: A solution (60 mL) of PVP (0.36 M, $M_n = 1.3 \times 10^6$ g mol^{-1}) in ethylene glycol was heated at 160 °C under constant stirring for 1 h to remove water from the solution. Next, a separate solution (30 mL) of silver nitrate in ethylene glycol ($AgNO_3$, 0.12 M) was prepared at room temperature by vigorous vortexing.[48] Sonication or heating was avoided, since it could

NANO MICRO small

lead to the unwanted formation of silver nanoparticles. Next, $Fe(acac)_3$ (50 μg) in ethylene glycol solution (0.5 mL) was added to the hot PVP solution, followed by dropwise addition of the homogeneous silver nitrate solution.[51] The dropwise addition was done manually by means of a pipette. The solution mixture was stirred for a minimum of 1 h, or until the solution turned opaque gray. The formation of AgNWs was easily confirmed by optical microscopy with 20× or 50× objectives, and was best observed in the dark-field mode.

AgNPl synthesis: A DMF solution (30 mL) of $AgNO_3$ (0.025 M) was added dropwise at room temperature to a stirred DMF solution of PVP (60 mL, 0.05 M, $M_n = 40\,000$ g mol^{-1}). The solution mixture gradually turned dark orange during the addition. The mixture was placed in an autoclave and then in a temperature-controlled oven at a constant temperature of 165 °C for 24 h.[52] The final product was tan-brown, and tended to aggregate into a mirrorlike film on the wall of the flask. Both AgNWs and AgNPls were purified from an excess of PVP by multiple centrifugation and redispersion cycles in methanol.

4-DMAP-coated gold nanoparticle synthesis: An aqueous solution (4.1 mL) of gold chloride ($HAuCl_4 \cdot HCl$, 30 mM) was mixed with a toluene solution (6.8 mL) of tetraoctylammonium bromide (TOAB, 25 mM) and vigorously stirred. As soon as all of the gold chloride salt was transferred from the aqueous phase into the organic phase, as seen from the distinctive yellow-orange color, a freshly prepared ice-cold aqueous solution (4.1 mL) of sodium borohydride ($NaBH_4$, 0.4 M) was added dropwise to the two-phase solution mixture. The solution gradually turned dark purple, almost black, accompanied by vigorous bubbling. The final solution mixture was stirred overnight. The next day, the purple organic phase was extracted with a pipette and washed with 0.1 M sulfuric acid, followed by 0.1 M sodium hydroxide, and finally washed three times with Nanopure water. An equal volume of an aqueous solution of 4-DMAP (0.1 M) was then added to the gold nanoparticle solution. Within 1 h, the gold nanoparticles moved into the aqueous phase. The aqueous phase was pipetted out and separated from the organic phase to give the Au:DMAP solution.

Attaching gold nanoparticles to AgNWs and AgNPls by electrostatics: AgNWs were easily isolated from a methanolic solution by brief centrifugation at 3300 rpm for less than 5 min. On the other hand, AgNPls required centrifugation at 5500 rpm for 20 min to completely isolate them from solution. To determine the silver nanoparticle concentration following centrifugation in preweighed centrifuge tubes, the transparent supernatant was pipetted out and the silver nanoparticle residue was dried in a vacuum to remove excess solvent. A typical concentration used for the subsequent procedures was 1–3 mg mL^{-1}.

To obtain negatively charged AgNWs, the AgNWs (10 mg) were mixed with 3-mercaptopropanoic acid overnight at a 1:10 mole ratio of silver atoms to 3-mercaptopropanoic acid in methanol at a concentration of 0.5 mg mL^{-1} (Scheme 1). The modified silver nanoparticles were isolated from excess ligands by multiple centrifugation–redispersion cycles in methanol. Finally, the silver nanoparticles were stored in phosphate buffer solution (pH 7) to activate the surface charge (1 mg mL^{-1} concentration, 10^{-5} M phosphate buffer). The AgNWs were dispersible in the buffer solution when sonicated or vortexed, but gradually precipitated within 30 min.

The gold nanoparticle densities on silver nanoparticle substrates were varied as follows. To obtain a low density of gold nanoparticles, a solution (0.1 mL) of the as-prepared Au:DMAP was diluted in Nanopure water (2.4 mL, pH 7, 2×10^{-3} M phosphate buffer). Next, this solution mixture was added dropwise to a stirred solution (2.5 mL) of negatively charged silver nanoparticles (1 mg mL^{-1} concentration, pH 7, 2×10^{-3} M phosphate buffer). The solution mixture was sonicated for 30 s and vortexed for 2 min to ensure uniform gold nanoparticle attachment onto the silver nanoparticle surfaces. Excess unattached gold nanoparticles were then removed by centrifugation (3300 rpm, 5 min). The silver–gold nanoparticle residue was then redispersed in a PAA solution (2 mg mL^{-1}, 0.01 M phosphate buffer) with the aid of brief sonication and vortexing (0.5 mg mL^{-1} concentration). Excess of unattached PAA was removed by multiple centrifugation and redispersion cycles in Nanopure water. This was to coat the outer silver–gold nanostructure with PAA (Scheme 1). Otherwise, the silver–gold nanoparticles were not dispersible in water. For a high density of gold nanoparticles, a solution (0.5 mL) of the as-prepared Au:DMAP was used instead for the same amount of silver nanoparticles. Correspondingly, a fivefold phosphate buffer concentration was used.

Silicon wafers were purchased from Semiconductor Processing Co. They were cut into 1.5×3 cm^2 pieces and sonicated in the presence of an aqueous solution of cetyltrimethylammonium bromide (CTAB, 1 wt% solution) to remove silicon dust. Next, they were rinsed multiple times with Nanopure water (Nanopure, 18.2 MΩ cm) before being submerged for 1 h in piranha solution (30% hydrogen peroxide, 70% concentrated sulfuric acid; *Caution!*) to remove organic contaminants. Finally, they were rinsed with abundant Nanopure water and dried with a nitrogen stream.[53]

Methods: Optical spectra were collected with a UV-2450 spectrophotometer (Shimadzu) and Craig point-short spectrophotometer on a Leica DM4000 microscope. An Alpha 300R Witec confocal Raman microscope was utilized to collect Raman spectra using an argon laser at $\lambda = 514.5$ nm. At least ten independent UV/Vis spectra were obtained for a single silver–gold nanowire using the Craig point-short spectrophotometer. The spectra were averaged, smoothed, and deconvoluted on Origin software. At 100× objective, the power was measured directly with a Thornlab power meter and adjusted to 70–80 μW. The integration time was set at 1 s. Raman maps were obtained within 1630–1680 cm^{-1} at 25×25 pixel^2 resolutions.

AFM topographical and phase images were obtained by using a Dimension-3000 atomic force microscope in the tapping mode at 1.0–2.0 Hz scan rate, according to the usual procedure.[54] Silicon nitride tips with radii between 30 and 60 nm and spring constants between 0.01 and 50 N m^{-1} were used. Langmuir–Blodgett films of AgNWs and AgNPls were obtained on a KSV 2000 minitrough according to the procedures described in the literature.[48,55,56] The purified nanostructures were centrifuged and redispersed in chloroform to give a concentration of approximately 10 mg mL^{-1}. A solution (150 μL) of the nanostructures was uniformly dispersed on a water surface and subjected to compression after 30 min to allow evaporation of chloroform and even distribution of silver nanoparticles. Densely packed monolayers were obtained at surface pressure $p = 30$ mN m^{-1} and transferred onto piranha-cleaned silicon

wafers. For SERS measurements, nanoparticle samples drop-cast onto piranha-cleaned silicon substrates were incubated in an aqueous solution of Rh6G ($10^{-4} < C_0 < 10^{-10}$ M) for 10 min.

Acknowledgements

The authors thank Dr. Samuel Shian for valuable discussions. Funding from NSF-DMR grant 0756273 and NSF-NIRT grant 0650705 is gratefully acknowledged.

[1] J. Zhang, X. Li, X. Sun, Y. Li, *J. Phys. Chem. B* **2005**, *109*, 12544.
[2] C. Burda, X. Chen, R. Narayanan, M. A. El-Sayed, *Chem. Rev.* **2005**, *105*, 1025.
[3] B. Zhang, H. Wang, L. Lu, K. Ai, G. Zhang, X. Cheng, *Adv. Funct. Mater.* **2008**, *18*, 2348.
[4] Y. Sun, Y. Xia, *Analyst* **2003**, *128*, 686.
[5] P. K. Jain, X. Huang, I. H. El-Sayed, M. A. El-Sayed, *Plasmonics* **2007**, *2*, 107.
[6] Y. Yang, S. Matsubara, M. Nogami, J. Shi, W. Huang, *Nanotechnology* **2006**, *17*, 2821.
[7] H. Ko, S. Singamaneni, V. V. Tsukruk, *Small* **2008**, *4*, 1576.
[8] N. R. Jana, T. Pal, *Adv. Mater.* **2007**, *19*, 1761.
[9] a) H. Xu, E. J. Bjerneld, M. Kall, L. Borjesson, *Phys. Rev. Lett.* **1999**, *83*, 4357; b) P. J. Moyer, J. Schmidt, L. M. Eng, A. J. Meixner, *J. Am. Chem. Soc.* **2000**, *122*, 5409; c) T. L. Haslett, L. Tay, M. Moskovits, *J. Chem. Phys.* **2000**, *113*, 1641.
[10] a) S. M. Nie, S. R. Emery, *Science* **1997**, *275*, 1102; b) K. Kneipp, Y. Wang, R. R. Dasari, M. S. Feld, *Appl. Spectrosc.* **1995**, *49*, 780; c) K. Kneipp, Y. Wang, H. Kneipp, L. T. Perelman, I. Itzkan, R. R. Dasari, M. Feld, *Phys. Rev. Lett.* **1997**, *78*, 1667; d) S. M. Nie, W. Doering, *J. Phys. Chem. B* **2002**, *106*, 311.
[11] a) R. P. Van Duyne, in *Chemical and Biochemical Applications of Lasers*, Vol. *4*(Ed.: C. B. Moor), Academic Press, New York **1979**, pp. 101–185; b) M. Moskovits, *Rev. Mod. Phys.* **1985**, *47*, 783.
[12] A Campion,, J. E. Ivanecky, C. M. Child, III, M. C. Foster, *J. Am. Chem. Soc.* **1995**, *117*, 11807.
[13] X.-M. Qian, S. M. Nie, *Chem. Soc. Rev.* **2008**, *37*, 912.
[14] J. B. Lassiter, J. Aizpurua, L. I. Hernandez, D. W. Brandl, I. Romero, S. Lai, J. H. Harfner, P. Nordlander, N. J. Halas, *Nano Lett.* **2008**, *8*, 1212.
[15] W. Huang, W. Qian, P. K. Jain, M. A. El-Sayed, *Nano Lett.* **2007**, *7*, 3227.
[16] P. K. Jain, W. Huang, M. A. El-Sayed, *Nano Lett.* **2007**, *7*, 2080.
[17] V. S. Tiwari, T. Oleg, G. K. Darbha, W. Hardy, J. P. Singh, P. C. Ray, *Chem. Phys. Lett.* **2007**, *446*, 77.
[18] S. E. Hunyadi, C. J. Murphy, *J. Mater. Chem.* **2006**, *16*, 3929.
[19] P. K. Jain, S. Eustis, M. A. El-Sayed, *J. Phys. Chem. B* **2006**, *110*, 18243.
[20] P. K. Jain, M. A. El-Sayed, *J. Phys. Chem. C* **2008**, *112*, 4954.
[21] S. T. Vidhu, O. Tovmachenko, K. D. Gopala, H. William, J. P. Singh, C. R. Paresh, *Chem. Phys. Lett.* **2007**, *446*, 77.
[22] S. L. Westcott, S. J. Oldenburg, T. R. Lee, N. J. Halas, *Chem. Phys. Lett.* **1999**, *300*, 651.
[23] H. Wang, D. W. Brandl, F. Le, P. Nordlander, N. J. Halas, *Nano Lett.* **2006**, *6*, 827.
[24] S. Xu, B. Zhao, W. Xu, Y. Fan, *Colloids Surf. A* **2005**, *257*, 313.
[25] W. Wang, C. Ruan, B. Gu, *Anal. Chim. Acta* **2006**, *567*, 121.
[26] M. Becker, V. Sivakov, U. Gösele, T. Stelzner, G. Andrä, H. J. Reich, S. Hoffmann, J. Michler, S. H. Christiansen, *Small* **2008**, *4*, 398.
[27] S. J. Lee, J. M. Baik, M. Moskovits, *Nano Lett.* **2008**, *8*, 3244.
[28] P.-P. Fang, J.-F. Li, S.-L. Yang, L.-M. Li, B. Ren, Z.-Q. Tian, *J. Raman Spectrosc.* **2008**, *39*, 1679.
[29] R. Gunawidjaja, S. Peleshanko, H. Ko, V. V. Tsukruk, *Adv. Mater.* **2008**, *20*, 1544.
[30] a) X. Li, S. He, *Nanotechnology* **2008**, *19*, 355501; b) S. Vial, I. Pastoriza-Santos, J. Perez-Juste, L. M. Liz-Marzan, *Langmuir* **2007**, *23*, 4606; c) H. Ding, K.-T. Yong, I. Roy, H. E. Pudavar, W. C. Law, E. J. Bergey, P. N. Prasad, *J. Phys. Chem. C* **2007**, *34*, 12552.
[31] a) A. P. Leonov, J. Zheng, J. D. Clogston, S. T. Stern, A. K. Patri, A. Wei, *ACS Nano* **2008**, *2*, 2481; b) H. Y. Koo, W. S. Choi, D.-Y. Kim, *Small* **2008**, *4*, 742; c) A. Gole, C. J. Murphy, *Langmuir* **2005**, *21*, 10756; d) C. Jiang, V. V. Tsukruk, *Soft Matter* **2005**, *1*, 334.
[32] H. Ko, S. Chang, V. V. Tsukruk, *ACS Nano* **2009**, *3*, 181.
[33] H. Ko, V. V. Tsukruk, *Small*, **2008**, *4*, 1980.
[34] S. Chang, H. Ko, S. Singamaneni, R. Gunawidjaja, V. V. Tsukruk, *Anal. Chem.* **2009**, *81*, 5740.
[35] C. Chen, L. Wang, G. Jiang, J. Zhou, X. Chen, H. Yu, Q. Yang, *Nanotechnology* **2006**, *17*, 3933.
[36] G. Schider, J. R. Krenn, A. Hohenau, H. Ditlbacher, A. Leitner, F. R. Aussenegg, *Phys. Rev. B* **2003**, *68*, 155427.
[37] A. Brioude, M. P. Pileni, *J. Phys. Chem. B* **2005**, *109*, 23371.
[38] C. Jiang, S. Markutsya, V. V. Tsukruk, *Langmuir* **2004**, *3*, 882.
[39] L. Gunnarsson, T. Rindzevicius, J. Prikulis, B. Kasemo, M. Käll, S. Zou, G. C. Schatz, *J. Phys. Chem. B* **2005**, *109*, 1079.
[40] R.-L. Zong, J. Zhou, Q. Li, B. Du, B. Li, M. Fu, X.-W. Qi, L. T. Li, S. Buddhudu, *J. Phys. Chem. B* **2004**, *108*, 16713.
[41] P. Hildenbrandt, M. Stockburger, *J. Phys. Chem.* **1984**, *88*, 5935.
[42] P. Mohanty, I. Yoon, T. Kang, K. Seo, K. S. K. Varadwaj, W. Choi, Q.-H. Park, J. P. Ahn, T. D. Suh, H. Ihlee, B. Kim, *J. Am. Chem. Soc.* **2007**, *129*, 9576.
[43] I. Yoon, T. Kang, W. Choi, J. Kim, Y. Yoo, S.-W. Joo, Q.-H. Park, H. Ihlee, B. Kim, *J. Am. Chem. Soc.* **2009**, *131*, 758.
[44] D. H. Jeong, Y. X. Zhang, M. Moskovits, *J. Phys. Chem. B* **2004**, *108*, 12724.
[45] P. Hildenbrandt, M. Stockburger, *J. Phys. Chem.* **1984**, *88*, 5935.
[46] A. R. Tao, P. Yang, *J. Phys. Chem. B* **2005**, *109*, 15687.
[47] B. Wiley, Y. Sun, Y. Xia, *Langmuir* **2005**, *21*, 8077.
[48] A. Tao, F. Kim, C. Hess, J. Goldberger, R. He, Y. Sun, Y. Xia, P. Yang, *Nano Lett.* **2003**, *3*, 1229.
[49] J. Zhang, X. Li, X. Sun, Y. Li, *J. Phys. Chem. B* **2005**, *109*, 12544.
[50] M. Brust, D. Bethell, D. J. Schiffrin, C. J. Kiely, *Adv. Mater.* **1995**, *7*, 795.
[51] B. Wiley, Y. Sun, Y. Xia, *Langmuir* **2005**, *21*, 8077.
[52] J. Zhang, X. Li, X. Sun, Y. Li, *J. Phys. Chem. B* **2005**, *109*, 12544.
[53] V. V. Tsukruk, V. N. Bliznyuk, *Langmuir* **1998**, *14*, 446.
[54] a) V. V. Tsukruk, *Rubber Chem. Technol.* **1997**, *70*, 430; b) V. V. Tsukruk, D. H. Reneker, *Polymer* **1995**, *36*, 1791.
[55] A. Tao, P. Sinsermsuksakul, P. Yang, *Nature* **2007**, *2*, 435.
[56] R. Gunawidjaja, H. Ko, C. Jiang, V. V. Tsukruk, *Chem. Mater.* **2007**, *19*, 2007.

Received: April 24, 2009
Revised: June 22, 2009
Published online: July 29, 2009

